

A guided residual search for nonlinear state-space identification*

Merijn Floren^{1,2} and Jan Swevers^{1,2}

Abstract—Parameter estimation of nonlinear state-space models from input-output data typically requires solving a highly non-convex optimization problem prone to slow convergence and suboptimal solutions. This work improves the reliability and efficiency of the estimation process by decomposing the overall optimization problem into a sequence of tractable subproblems. Based on an initial linear model, nonlinear residual dynamics are first estimated via a guided residual search and subsequently refined using multiple-shooting optimization. Experimental results on two benchmarks demonstrate competitive performance relative to state-of-the-art black-box methods and improved convergence compared to naive initialization.

Index Terms—Nonlinear systems identification, identification for control, optimization

I. INTRODUCTION

Identifying nonlinear dynamical systems from experimental input-output data is challenging because it requires both model structure selection and parameter estimation. These aspects are strongly coupled, as a carefully chosen structured representation can greatly facilitate parameter estimation.

State-space models provide a natural framework for this task, as they closely reflect the underlying physics while allowing structural constraints to be imposed. Among state-space formulations, the *nonlinear linear fractional representation* (NL-LFR) framework offers a principled decomposition in which dominant linear dynamics are separated from localized nonlinearities through a feedback interconnection between a linear time-invariant (LTI) system and a static nonlinearity, as illustrated in Fig. 1. This formulation captures a wide range of nonlinear phenomena while retaining sufficient structure for efficient parameter estimation.

In this work, the focus is on estimating simulation models. This typically requires solving a highly nonlinear and non-convex optimization problem in the model parameters, which is prone to poor local minima and sensitive to initialization. Recursive simulation further introduces vanishing and exploding gradient effects, increasing computational cost. These challenges become more pronounced with longer horizons and more complex models, underscoring the need for robust and efficient optimization strategies.

Two main strategies have been proposed to address the parameter estimation problem. The first strategy aims to provide a favorable initialization, such that the solver starts near a desirable local minimum. This approach is adopted, for example, in [1], [2], where nonlinear state-space models are initialized from an estimated linear model. While this provides a reasonable starting point for optimization, the

*This work is supported by Flanders Make’s IRVA projects ASSISStANT and CoMoDO. ¹Department of Mechanical Engineering, KU Leuven, Belgium. ²Flanders Make@KU Leuven, Belgium. Corresponding author email: merijn.floren@kuleuven.be.

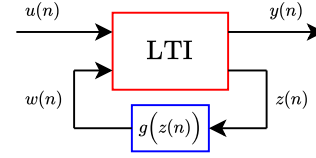


Fig. 1: Schematic overview of the NL-LFR structure.

parameters associated with the nonlinear residual remain randomly initialized, which may still lead to suboptimal solutions. A second strategy seeks to explicitly estimate part of the latent state trajectory. During optimization, the model is then simulated only over short horizons starting from these estimated states, which smooths the loss landscape [3]. However, accurate state estimation itself remains challenging.

Several approaches have been proposed to realize this second idea in practice. In [3], [4], the states are treated as decision variables for optimization, thereby introducing additional initialization requirements. A different strategy in [5] infers latent states using deep subspace encoders trained jointly with the nonlinear state-space model, which is computationally demanding due to the simultaneous training of both the encoder and the dynamical model. More recently, guided residual search methods have been introduced to efficiently estimate latent dynamics by exploiting the NL-LFR structure and available initial models [6], [7], [8], [9]. These methods, however, either rely on prior knowledge of the governing equations or assume periodic data, and inherently introduce a *distribution shift* between the residual estimation stage and the NL-LFR deployment stage.

In this work, we extend the guided residual search rationale to identifying general NL-LFR models from arbitrary input-output data. In contrast to [7], [8], [9], the proposed method does not require prior knowledge of the system’s underlying physical equations, and unlike [6], [7], [8], it does not require periodic data. Furthermore, the distribution shift affecting these methods is theoretically established and experimentally demonstrated for the first time, and a corresponding mitigation strategy is proposed.

The remainder of this paper is structured as follows. Section II establishes the problem context, while Section III presents the proposed identification approach. Section IV demonstrates the method’s effectiveness on two experimental benchmark datasets, and Section V concludes the paper.

Notation. The sets of real, integer, and natural numbers are denoted by \mathbb{R} , \mathbb{Z} , and \mathbb{N} , respectively. For $x \in \mathbb{R}^n$ and symmetric positive definite $Q \in \mathbb{R}^{n \times n}$, define $\|x\|_Q^2 = x^\top Q x$, and $\|x\|^2 = x^\top x$, where $(\cdot)^\top$ denotes the transpose. The identity matrix is denoted by I , and 0 denotes the zero matrix, with dimensions clear from context.

II. PROBLEM STATEMENT

The adopted NL-LFR structure is parametrized as:

$$x(n+1) = Ax(n) + B_u u(n) + B_w w(n), \quad (1a)$$

$$y_0(n) = C_y x(n) + D_{yu} u(n) + D_{yw} w(n), \quad (1b)$$

$$z(n) = C_z x(n) + D_{zu} u(n), \quad (1c)$$

$$w(n) = f_{\text{NN}}(z(n)), \quad (1d)$$

where $x(n) \in \mathbb{R}^{n_x}$ denotes the latent state at time index $n \in \mathbb{Z}$, $u(n) \in \mathbb{R}^{n_u}$ and $y_0(n) \in \mathbb{R}^{n_y}$ denote the exact input and output, respectively, and $z(n) \in \mathbb{R}^{n_z}$ and $w(n) \in \mathbb{R}^{n_w}$ denote the respective input and output of the nonlinearity. The matrices $A \in \mathbb{R}^{n_x \times n_x}$, $B_u \in \mathbb{R}^{n_x \times n_u}$, $B_w \in \mathbb{R}^{n_x \times n_w}$, $C_y \in \mathbb{R}^{n_y \times n_x}$, $C_z \in \mathbb{R}^{n_z \times n_x}$, $D_{yu} \in \mathbb{R}^{n_y \times n_u}$, $D_{yw} \in \mathbb{R}^{n_y \times n_w}$, and $D_{zu} \in \mathbb{R}^{n_z \times n_u}$ define the LTI dynamics. The static nonlinearity $f_{\text{NN}} : \mathbb{R}^{n_z} \rightarrow \mathbb{R}^{n_w}$ is parametrized as a feedforward neural network with n_l hidden layers:

$$\begin{aligned} z^{[l]}(n) &= \sigma(W^{[l]} z^{[l-1]}(n) + b^{[l]}), \quad l = 1, \dots, n_l, \\ w(n) &= W^{[n_l+1]} z^{[n_l]}(n) + b^{[n_l+1]}, \end{aligned} \quad (2)$$

where $\sigma(\cdot)$ denotes an elementwise nonlinear activation function, and $z^{[0]}(n) = z(n)$. The weight matrices $W^{[l]}$ and bias vectors $b^{[l]}$, of appropriate dimensions, are collectively denoted by the parameter set $\theta_{\text{NN}} = \{W^{[l]}, b^{[l]}\}_{l=1}^{n_l+1}$.

Assumption 1. The measured output is corrupted by additive, zero-mean, stationary noise $v(n)$ with finite variance, i.e., $y(n) := y_0(n) + v(n)$. The noise may be colored and is uncorrelated with the input $u(n)$, which is exactly known.

Assumption 2. The input signal $u(n)$ is persistently exciting of a sufficiently high order.

For parameter estimation, we consider a dataset of N input-output samples, collected from the system under test:

$$\mathcal{D} = \{(u(n), y(n))\}_{n=0}^{N-1}, \quad (3)$$

where both $u(n)$ and $y(n)$ are normalized to have zero mean and unit variance. To focus on the core contributions, the method starts from an initial linear model $\mathcal{M}_0 = (\hat{A}, \hat{B}_u, \hat{C}_y, \hat{D}_{yu})$ that is stable and provides a rough approximation of the linear input-output behavior of the system.

We propose a sequential identification strategy consisting of three stages. Specifically, (i) a guided residual search is performed to infer the latent variables w and x while simultaneously estimating the matrices B_w and D_{yw} ; (ii) the neural network f_{NN} is trained, together with the matrices C_z and D_{zu} , using the inferred latent variables; and (iii) all model parameters are jointly refined through nonlinear optimization. Steps (i) and (ii) aim to accelerate convergence of step (iii) by providing a well-informed initialization, but also introduce their own challenge, discussed next.

A. Mitigating distribution shift using multiple shooting

The second stage of the proposed strategy estimates the parameters associated with the nonlinear residual under a formulation that intentionally ignores the recursive state evolution in (1a), i.e., the inferred samples from the guided residual search are treated as temporally independent. This decoupling is highly beneficial from an optimization perspective, but holds only during this specific training stage. When

the learned model is later deployed for forward simulation, the recursive structure of (1a) is restored, causing each neural network output to influence its own future inputs through the state dynamics. This recursive feedback allows small modeling inaccuracies to accumulate over time, introducing a distribution shift between the training and simulation environments, that may quickly lead to divergence. Building on [10], [3], we formalize this phenomenon as follows.

Theorem 1. Let $x(n+1) = f(x(n), u(n))$ denote the unified state-update equation corresponding to (1a), (1c), and (1d), learned in a one-step fashion from the samples $\{x(n), u(n)\}_{n=0}^{N-1}$. Moreover, assume $f : \mathbb{R}^{n_x} \times \mathbb{R}^{n_u} \rightarrow \mathbb{R}^{n_x}$ is uniformly Lipschitz continuous in x with constant $L > 1$, i.e., $\|f(x_1, u) - f(x_2, u)\| \leq L\|x_1 - x_2\|$ for all $x_1, x_2 \in \mathbb{R}^{n_x}$, $u \in \mathbb{R}^{n_u}$, and that the one-step prediction error is uniformly bounded, i.e., $\|f(x(n), u(n)) - x(n+1)\| \leq \varepsilon$ for all $n \in \{0, \dots, N-2\}$. Then, by recursively feeding the simulated states $\hat{x}(n+1) = f(\hat{x}(n), u(n))$ back into $f(\cdot)$, with $\hat{x}(0) = x(0)$, the resulting simulation error at the final time sample satisfies $\|\hat{x}(N-1) - x(N-1)\| \in \mathcal{O}(L^{N-1}\varepsilon)$.

Proof: Define the simulation error as $e_n := \hat{x}(n) - x(n)$. Then $e_{n+1} = f(\hat{x}(n), u(n)) - x(n+1)$. Inserting $f(x(n), u(n))$ twice and applying the triangle inequality yields $\|e_{n+1}\| \leq \|f(\hat{x}(n), u(n)) - f(x(n), u(n))\| + \|f(x(n), u(n)) - x(n+1)\|$. By Lipschitz continuity and the one-step prediction bound, we obtain $\|e_{n+1}\| \leq L\|e_n\| + \varepsilon$. With $e_0 = 0$, iterating this recursion gives $\|e_{N-1}\| \leq \varepsilon \sum_{n=0}^{N-2} L^n$. If $L \neq 1$, the geometric sum equals $\frac{L^{N-1}-1}{L-1}$, implying $\|e_{N-1}\| \in \mathcal{O}(L^{N-1}\varepsilon)$ for $L > 1$. ■

Theorem 1 states that, when the nonlinear residual is parametrized as proposed, prediction errors may grow exponentially during simulation, thereby negating its intended beneficial effect. Note that we assume $L > 1$, since $f(\cdot)$ is partly implemented using a neural network, which typically has a Lipschitz constant greater than one [11], [12].

To account for accumulating simulation errors, we use multiple shooting [13] in the final optimization stage. Multiple shooting divides the simulation into shorter intervals, with the initial state of each interval treated as a decision variable. The shorter intervals improve convergence by limiting error accumulation, smoothing the loss landscape, and enabling recovery from non-contractive parameter regions [3], [4]. In practice, these benefits still depend on good initialization of the many decision variables. Our approach naturally provides this initialization by using the states and model parameters obtained in the preceding steps.

III. METHODOLOGY

A. Bilevel guided residual search

In this first step, the model \mathcal{M}_0 is held fixed, and the dual objective is to parametrize $\theta_{wy} := (B_w, D_{yw})$ and infer the latent variables w and x , used to train the neural network in Section III-B. To this end, we propose a bilevel optimization scheme with two alternating stages: (i) an inner problem that estimates w and x conditioned on θ_{wy} , and (ii) an outer problem that updates θ_{wy} based on the inferred signals.

1) *Inner problem:* Consider the fully parametrized submodel \mathcal{M}_1 defined by (1a) and (1b), in which w is treated as an exogenous input. The fixed matrices A , B_u , C_y , and D_{yu} of \mathcal{M}_1 , in that order, are obtained by applying a similarity transformation to \mathcal{M}_0 , yielding

$$\theta_{uy} := (T_x^{-1}\hat{A}T_x, T_x^{-1}\hat{B}_u, \hat{C}_yT_x, \hat{D}_{yu}), \quad (4)$$

where T_x is diagonal and constructed from the empirical standard deviations of the simulated state trajectories of \mathcal{M}_0 . This transformation normalizes the state variables to have approximately unit variance, which is beneficial for all subsequent optimization stages.

The objective of this inner problem is to obtain a nonparametric estimate of w that minimizes the discrepancy between the simulated outputs of \mathcal{M}_1 and the measured outputs in \mathcal{D} . For this purpose, we employ a sliding window strategy, in which w is estimated by solving a local optimization problem over a finite time window of length $H + 1 \ll N$, where $H \in \mathbb{N}$ denotes the prediction horizon length. Only the solution corresponding to the first time instance is retained and used to shift the window forward in time. Along the way, the latent state x is naturally inferred as well.

Assumption 3. The submodel \mathcal{M}_1 is output controllable with respect to its exogenous input w .

Remark 1. Using a windowed approach, rather than relying on instantaneous or one-step-ahead estimates of w , reduces sensitivity to measurement noise in \mathcal{D} , as the influence of individual noisy samples is averaged over time.

In the following, the explicit dependence on θ_{wy} is omitted for notational clarity. For $s \in \{u, w, y\}$, we first define

$$\mathcal{S}_s(n) = \begin{bmatrix} s(n) \\ s(n+1) \\ \vdots \\ s(n+H) \end{bmatrix} \in \mathbb{R}^{n_s(H+1)}. \quad (5)$$

Then, for each $n \in \{0, \dots, N - H - 1\}$, we solve:

$$\min_{\mathcal{S}_w(n)} \frac{1}{2} \|\mathcal{S}_y(n) - \hat{\mathcal{Y}}(n)\|^2 + \frac{\lambda}{2} \|\mathcal{S}_w(n)\|_{\Theta}^2, \quad (6a)$$

$$\text{s.t.} \quad \hat{\mathcal{Y}}(n) = \mathcal{O}_x x_*(n) + \mathcal{T}_u \mathcal{S}_u(n) + \mathcal{T}_w \mathcal{S}_w(n), \quad (6b)$$

where $\lambda \in \mathbb{R}_{>0}$ represents a regularization hyperparameter that balances the trade-off between output fit and solution variability by penalizing the influence of $\mathcal{S}_w(n)$ on the state and output predictions through

$$\Theta = \begin{bmatrix} B_w \\ D_{yw} \end{bmatrix}^\top \begin{bmatrix} B_w \\ D_{yw} \end{bmatrix} + \frac{\epsilon}{\lambda} I, \quad (7)$$

with $\epsilon \in \mathbb{R}_{>0}$ a small constant ensuring strict positive definiteness. The stacked output predictions in (6b) are expressed using the extended observability matrix

$$\mathcal{O}_x = [(C_y)^\top \quad (C_y A)^\top \quad \dots \quad (C_y A^H)^\top]^\top, \quad (8a)$$

of size $n_y(H+1) \times n_x$, and the block Toeplitz matrices

$$\mathcal{T}_v = \begin{bmatrix} D_{yv} & 0 & \dots & 0 \\ C_y B_v & D_{yv} & \dots & 0 \\ \vdots & \vdots & \ddots & \vdots \\ C_y A^{H-1} B_v & C_y A^{H-2} B_v & \dots & D_{yv} \end{bmatrix}, \quad (8b)$$

for $v \in \{u, w\}$, with $\mathcal{T}_v \in \mathbb{R}^{n_y(H+1) \times n_v(H+1)}$. The optimization problem in (6) is convex, with closed-form solution:

$$\mathcal{S}_{w_*}(n) = -\mathcal{G}^{-1} \mathcal{T}_w^\top (\mathcal{O}_x x_*(n) + \mathcal{T}_u \mathcal{S}_u(n) - \mathcal{S}_y(n)), \quad (9)$$

where $\mathcal{G} = \mathcal{T}_w^\top \mathcal{T}_w + \lambda \Theta$. The first n_w elements of $\mathcal{S}_{w_*}(n)$ are retained as $w_*(n)$ and used to advance the window forward in time according to

$$x_*(n+1) = Ax_*(n) + B_u u(n) + B_w w_*(n). \quad (10)$$

Here, $x_*(0)$ is set to zero, thereby inducing a transient response that is unsuitable for parametric modelling of the nonlinear residual. Therefore, the first $N_0 \in \mathbb{N}$ samples of each realization are later discarded, finally leading to

$$\mathcal{D}_* = \{(w_*(n), x_*(n), y_*(n))\}_{n=N_0}^{N-H-1}, \quad (11)$$

where $y_*(n)$ is computed according to (1b).

2) *Outer problem:* The dataset \mathcal{D}_* is obtained each time the inner problem is solved, conditioned on the current estimate of θ_{wy} , whose initial values are drawn from $\mathcal{U}(-1, 1)$. The parameters θ_{wy} are then updated through:

$$\min_{\theta_{wy}} \frac{1}{N_{\text{tot}}} \sum_{n=N_0}^{N-H-1} \|y(n) - y_*(n | \theta_{wy})\|^2, \quad (12)$$

where $N_{\text{tot}} = N - H - N_0$. The bilevel scheme alternates between the inner and outer problems until convergence.

Remark 2. The outcome of the guided residual search is sensitive to the random initialization of θ_{wy} , as typical initializations render \mathcal{M}_1 output controllable with respect to w . This dependence introduces multiple effective minimizers of the outer loss (12), not all yielding meaningful relationships between x and w . Especially for high-dimensional systems, multiple initializations should therefore be considered, with the neural network trained on each inferred dataset.

B. Parametric learning of the nonlinear residual

The objective of this second step is to learn the nonlinear residual parameters $\theta_{\text{nl}} := (C_z, D_{zu}, \theta_{\text{NN}})$ from \mathcal{D}_* obtained at convergence of the guided residual search. The matrices C_z and D_{zu} are initialized with elements drawn from $\mathcal{U}(-1, 1)$, while θ_{NN} is initialized using the Xavier method [14]. The parameters θ_{nl} are then learned by minimizing the following loss:

$$\min_{\theta_{\text{nl}}} \frac{1}{N_{\text{tot}}} \sum_{n=N_0}^{N-H-1} \|w_*(n) - \hat{w}_*(n | \theta_{\text{nl}})\|^2, \quad (13)$$

where $\hat{w}_*(n | \theta_{\text{nl}}) = f_{\text{NN}}(C_z x_*(n) + D_{zu} u(n))$. Note that, by implicitly treating the samples in \mathcal{D}_* as independent and identically distributed, the optimization problem (13) can be solved efficiently using parallel GPU computation.

C. Final optimization using multiple shooting

In this final stage, we have (i) an NL-LFR model with parameters $\theta := (\theta_{uy}, \theta_{wy}, \theta_{\text{nl}})$, initialized using the results of the preceding steps, and (ii) state estimates obtained from the guided residual search. This setup establishes a fully initialized multiple-shooting problem with both parameters and shooting states as decision variables. Specifically, the starting indices of the shooting intervals are defined as

$$\mathcal{I} := \{N_0 + id \mid i \in \{0, \dots, \lfloor (N_{\text{tot}} - 1)/d \rfloor\}\}, \quad (14)$$

where $d \geq 1$ denotes the interval length and $\lfloor \cdot \rfloor$ is the floor function. The corresponding shooting states are defined as

$$\mathcal{X} := \{x(n) \mid n \in \mathcal{I}\}, \quad (15)$$

with their initial values taken from the state estimates obtained from \mathcal{D}_* . State propagation within each interval is enforced over the index set

$$\mathcal{N}_i := \{i, \dots, \min(i + d - 1, N - H - 1)\}, \quad i \in \mathcal{I}. \quad (16)$$

Finally, let \mathcal{I}^- denote the set of all but the last indices in \mathcal{I} . Then, the multiple-shooting problem becomes:

$$\min_{\theta, \mathcal{X}} \frac{1}{N_{\text{tot}}} \sum_{n=N_0}^{N-H-1} \|y(n) - \hat{y}(n \mid \theta, \mathcal{X})\|^2, \quad (17a)$$

$$\text{s.t.} \quad \hat{x}(n) = x(n), \quad n \in \mathcal{I}, \quad (17b)$$

$$\hat{x}(n+1) = f(\hat{x}(n), u(n)), \quad n \in \mathcal{N}_i, i \in \mathcal{I}, \quad (17c)$$

$$\hat{y}(n) = h(\hat{x}(n), u(n)), \quad n \in \mathcal{N}_i, i \in \mathcal{I}, \quad (17d)$$

$$\hat{x}(n+d) = x(n+d), \quad n \in \mathcal{I}^-, \quad (17e)$$

with $f(\cdot)$ and $h(\cdot)$ denoting the unified state-update and output equations, respectively, according to (1). Continuity of the state trajectory across the intervals is ensured by (17e).

IV. RESULTS

We evaluate the proposed method on two experimental benchmarks: the Silverbox system [15] and a ground vibration test of an F-16 fighter aircraft [16]. All computations are performed in Python on a 2.3 GHz Intel Core i7 with 16 GB RAM. As both datasets are periodic, the respective initial linear models are parametrized using the *best linear approximation* (BLA), following the exact procedure in [6]; subsequent steps do not exploit periodicity. The guided residual search and neural network training are implemented in JAX [17], using solvers from Optax [18] and Optimistix [19]. Multiple-shooting optimization is implemented in CasADi [20] using the IPOPT solver.

A. Silverbox benchmark system

The Silverbox system [15] represents an electronic implementation of a mass-spring-damper system with a cubic spring nonlinearity. In the benchmark dataset, the input voltage is analogous to the applied force and the output voltage to the displacement. The resulting input-output data exhibit an arrow-shaped structure consisting of two segments, sampled at approximately 610 Hz. The first segment (“arrowhead”, used for testing) contains 40 000 samples of white Gaussian noise with linearly varying amplitude, filtered by a 9th-order Butterworth filter with cutoff frequency 200 Hz. The second segment consists of 86 750 samples corresponding to ten random-phase multisine realizations, exciting only odd harmonics up to 200 Hz, of which the final 21 688 samples are reserved for testing.

1) *Algorithmic performance*: The objective of this first analysis is to assess the benefits of the guided residual search and compare multiple- and single-shooting optimization strategies. We consider the following four scenarios:

S1 *Multiple shooting with guided residual search*. The procedure in Section III is applied with $n_x = 2$ and $n_w = n_z = 1$. The guided residual search uses $H = 10$,

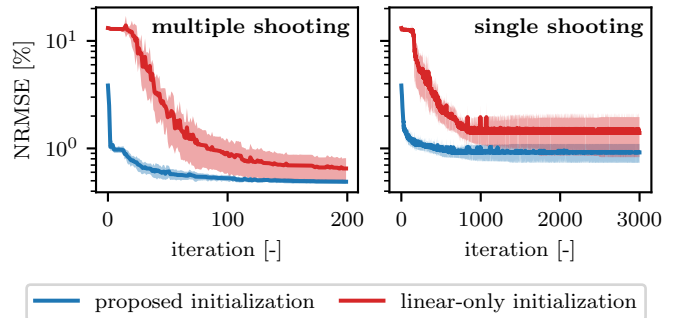


Fig. 2: NL-LFR simulation NRMSEs over the iterations of the final optimization stage, for Silverbox scenarios **S1** to **S4**. The guided residual search provides a favorable initialization, and multiple shooting outperforms single shooting.

$N_0 = 100$, $\lambda = 1$, and $\epsilon = 10^{-8}$ for 25 Levenberg-Marquardt iterations. The neural network consists of a single hidden layer with 15 ReLU neurons and is trained for 100 Adam iterations with learning rate 10^{-3} . Multiple shooting uses $d = 1$ for 200 IPOPT iterations.

S2 *Single shooting with guided residual search*. Identical initialization as in **S1**, followed by 3000 IPOPT iterations of single shooting¹, meaning that $d = N_{\text{tot}}$.

S3 *Multiple shooting with linear-only initialization*. The BLA model is normalized as in (4), and θ_{nl} is initialized according to Section III-B, using the same architecture and initialization as in **S1**. Yet, the matrices B_w and D_{yw} are initialized from $\mathcal{U}(-10^{-4}, 10^{-4})$, ensuring agreement with the BLA loss at the first iteration while avoiding zero gradients. The initial states for multiple shooting are obtained from simulated trajectories of the normalized BLA, and all other settings follow **S1**.

S4 *Single shooting with linear-only initialization*. Same initialization as in **S3**, followed by single-shooting optimization with the settings of **S2**.

We simulate each scenario 25 times, each with a different random initialization seed, and monitor the simulation performance of the NL-LFR models across iterations using the normalized root mean square error (NRMSE). The results are visualized in Fig. 2, where the solid lines represent the median performance and the shaded areas indicate their respective median absolute deviations. Here, the NRMSEs are computed over the full training set \mathcal{D} with the initial 100 samples discarded to exclude transient effects².

As expected, the guided residual search yields a lower initial NRMSE at the start of the shooting-based optimization, reflecting the benefit of proper initialization. The improved initialization also promotes consistent convergence to lower final NRMSE values, regardless of the shooting strategy. Moreover, scenarios **S1** and **S2** exhibit a steep initial descent,

¹Multiple shooting typically converges in fewer iterations than single shooting due to reduced non-convexity, but requires more computational effort per iteration. We therefore compare IPOPT iteration counts corresponding to roughly the same runtime on our CPU (about 20 minutes).

²For multiple shooting, the reported NRMSEs do not necessarily coincide with the loss function value, since the latter is computed over short intervals, while the NRMSEs are computed from recursive forward simulations. In contrast, for single shooting, the two quantities are directly related.

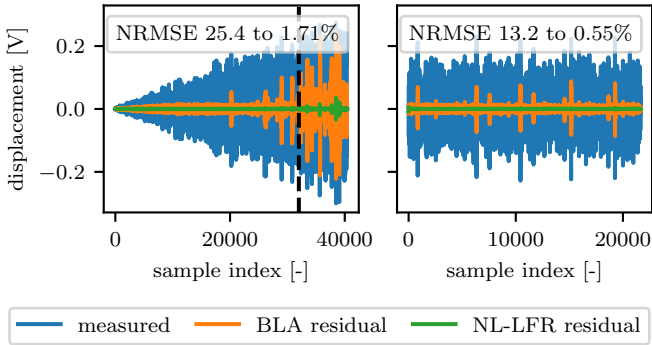


Fig. 3: Best-performing NL-LFR model from **S1** on the Silverbox arrowhead (left) and multisine (right) test data, compared to the BLA model. The dashed vertical line marks the start of the extrapolation region.

TABLE I: Simulation root mean square errors (RMSEs) on the Silverbox test data (mean \pm standard deviation in mV) for the NL-LFR models of **S1**, compared with state-of-the-art black-box methods.

	proposed	SUBNET [5]	PNLSS [1]
multisine	0.33 ± 0.02	0.36	-
arrowhead (full)	1.13 ± 0.15	1.40	0.26
arrowhead (no extrap.)	0.31 ± 0.03	0.32	-

whereas scenarios **S3** and **S4** show limited progress during the early iterations. These pronounced early improvements indicate that the parameters lie within a favorable attraction region, with the initial iterations primarily compensating for feedback effects neglected during neural network training. It is worth noting that the guided residual search plus neural network training required only 21 s on average, providing an attractive trade-off between initialization effort and downstream optimization performance. Figure 2 further demonstrates that multiple shooting outperforms single shooting, consistently converging to lower final NRMSE values regardless of the initialization approach. This behavior likely results from the smoothing effect of multiple shooting on the loss landscape and its gradients [3]. While already effective, the present implementation did not exploit the inherent parallelism of multiple shooting, which would further improve the computational efficiency.

2) *Test data performance*: The best-performing model from scenario **S1** is evaluated on the test data, as illustrated in Fig. 3. The resulting model accurately reproduces the system dynamics for both excitation signals and clearly outperforms the BLA. For the arrowhead signal, most of the error arises from extrapolation beyond the training domain, which is expected given the black-box nature of neural networks and their limited extrapolation capability.

Table I summarizes the RMSE test values of the models obtained from **S1**, alongside benchmark results from state-of-the-art black-box approaches: the SUBNET deep encoder [5] and the PNLSS method [1]. The proposed method performs competitively, with SUBNET exhibiting similar extrapolation errors on the arrowhead signal. In contrast, PNLSS achieves superior extrapolation due to its degree-three polynomial basis, consistent with the cubic system nonlinearity.

B. F-16 ground vibration test

The proposed method is then evaluated on a more complex F-16 ground vibration dataset [16], comprising one input and three outputs. Excitation is applied using an electrodynamic shaker mounted beneath the right wing, with accelerometers measuring the response near the payload interface and excitation point. A dummy payload attached to the wing tip introduces expected stiffness and damping nonlinearities. The estimation data consist of eight steady-state periods of a single random-phase multisine excitation spanning 2 Hz to 15 Hz, each containing 8192 samples and a root mean square (RMS) excitation amplitude of 73.6 N. Prior to identification, the periods are averaged, and the data are low-pass filtered at 15 Hz to reduce measurement noise. Based on empirical tuning, the model orders are selected as $n_x = 15$, $n_w = 2$, and $n_z = 6$. The guided residual search is performed with $H = 10$, $N_0 = 500$, $\lambda = 100$, and $\epsilon = 10^{-8}$ for 50 Levenberg-Marquardt iterations. The neural network consists of a single hidden layer with 32 neurons using hyperbolic tangent activation functions and is trained for up to 1000 Adam iterations with learning rate 4×10^{-3} .

In Section II-A, we established theoretically that the proposed sequential method may produce initial models for the final optimization stage with exponentially large simulation error due to distribution shift. To examine this effect experimentally, we track the deployment performance of the NL-LFR model throughout neural network training. Here, deployment performance is quantified by the simulation NRMSE, averaged over the three outputs, obtained if the full NL-LFR model were to be simulated after each training iteration. The neural network training performance is measured by the static loss defined in (13). The results, shown in Fig. 4, indicate that although the neural network loss (13) decreases monotonically, the simulation NRMSE rapidly deteriorates and exhibits pronounced volatility. This apparent discrepancy is consistent with Theorem 1, which states that simulation accuracy is exponentially sensitive to the Lipschitz constant L over extended rollouts, even when the one-step-ahead error bound ϵ is small. While neural network training reduces the one-step-ahead error on the training data, it typically leads to an increased Lipschitz

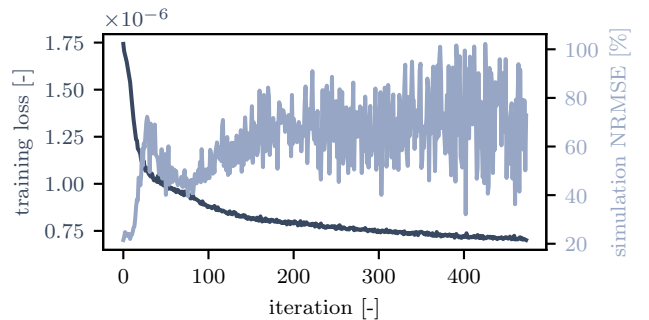


Fig. 4: Distribution shift over the F-16 neural network training iterations. The static neural network loss (13) steadily decreases, but the simulation error of the resulting NL-LFR model quickly deteriorates and exhibits high volatility.

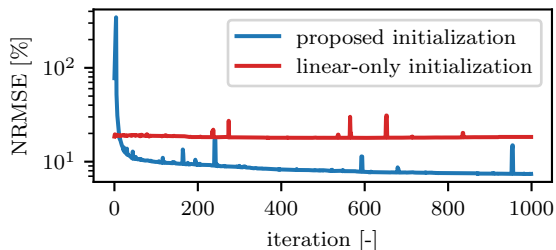


Fig. 5: F-16 simulation NRMSEs during the final optimization stage. Despite a higher initial error due to distribution shift (see Fig. 4), the proposed method starts in a favorable parameter region and converges rapidly, while the linear-only initialization is trapped in a local minimum.

TABLE II: Per-output simulation NRMSEs of the BLA and NL-LFR models evaluated on the F-16 test data.

	output 1	output 2	output 3
BLA	11.59 %	19.40 %	20.59 %
NL-LFR	9.20 %	12.55 %	13.27 %

constant [12]. The combined effect of these opposing trends may substantially degrade simulation accuracy.

We initialize the final optimization stage using the NL-LFR model obtained at the last iteration shown in Fig. 4. Although this model exhibits a higher simulation error than the initial linear model, this does not necessarily indicate an unfavorable parameter region. Moreover, simulation accuracy is less critical here, since the optimization is performed over shorter horizons. We track the multiple-shooting optimization over 1000 IPOPT iterations with an interval length of $d = 200$ samples³, and compare it to a linear-only initialization. The resulting simulation NRMSEs, averaged over the three outputs, are shown in Fig. 5. Although the linear model starts from a lower simulation error, it quickly becomes trapped in a local minimum and shows little further improvement. In contrast, the NL-LFR model, despite its poorer initial performance, improves rapidly and converges to a substantially better solution. Figure 5 thus demonstrates that initial NL-LFR models obtained via the sequential approach may lie in a favorable parameter region for subsequent optimization, even when their initial simulation error is high.

We finally assess the generalization performance of the optimized NL-LFR model on an unseen test dataset consisting of eight steady-state periods of the same random-phase multisine realization, applied at a higher amplitude of 85.7 N RMS. As with the training data, the periods are averaged and low-pass filtered at 15 Hz. Table II reports the per-output simulation NRMSEs compared to the BLA. The NL-LFR model achieves a clear improvement, although the increased excitation amplitude, system complexity, and limited training data result in some residual simulation error.

V. CONCLUSIONS

This work presented a novel time-domain identification approach for NL-LFR state-space models that decomposes the inherently non-convex optimization problem into a sequence

³Chosen as a compromise between memory usage and algorithm performance; $d = 1$ would offer best convergence but exceeds available memory.

of tractable subproblems. A key contribution is the guided residual search, which efficiently estimates the nonlinear residual dynamics but induces a distribution shift influencing the subsequent joint optimization; this shift was analyzed theoretically, illustrated experimentally, and effectively mitigated through a multiple-shooting strategy. Validation on two experimental benchmarks showed improved convergence over naive initialization and competitive performance compared to state-of-the-art black-box methods.

REFERENCES

- [1] J. Paduart, L. Lauwers, J. Swevers, K. Smolders, J. Schoukens, and R. Pintelon, "Identification of nonlinear systems using polynomial nonlinear state space models," *Automatica*, vol. 46, no. 4, 2010.
- [2] M. Schoukens and R. Tóth, "On the initialization of nonlinear LFR model identification with the best linear approximation," *IFAC-PapersOnLine*, vol. 53, no. 2, pp. 310–315, 2020.
- [3] A. H. Ribeiro, K. Tiels, J. Umenberger, T. B. Schön, and L. A. Aguirre, "On the smoothness of nonlinear system identification," *Automatica*, vol. 121, p. 109158, 2020.
- [4] A. Retzler, J. Swevers, J. Gillis, and Z. Kollár, "Shooting methods for identification of nonlinear state-space grey-box models," in *2022 IEEE 17th International Conference on Advanced Motion Control (AMC)*. IEEE, 2022, pp. 207–212.
- [5] G. Beintema, R. Tóth, and M. Schoukens, "Nonlinear state-space identification using deep encoder networks," in *Learning for Dynamics and Control*. PMLR, 2021, pp. 241–250.
- [6] M. Floren, J.-P. Noël, and J. Swevers, "Inference and learning of nonlinear LFR state-space models," *IEEE Control Systems Letters*, vol. 9, pp. 1345 – 1350, 2025.
- [7] M. Floren and J. Swevers, "A sliding-window approach for latent restoring force modeling," *arXiv:2602.21918*, 2026.
- [8] M. Floren and J.-P. Noël, "Nonlinear restoring force modelling using Gaussian processes and model predictive control," in *Conference Proceedings of ISMA2022-USD2022*, 2022, pp. 2493–2498.
- [9] M. Floren, S. Mamedov, J.-P. Noël, and J. Swevers, "Identification of deformable linear object dynamics from input-output measurements in 3D space," *IFAC-PapersOnLine*, vol. 58, no. 15, pp. 468–473, 2024.
- [10] A. Venkatraman, M. Hebert, and J. Bagnell, "Improving multi-step prediction of learned time series models," in *Proceedings of the AAAI Conference on Artificial Intelligence*, vol. 29, no. 1, 2015.
- [11] H. Gouk, E. Frank, B. Pfahringer, and M. J. Cree, "Regularisation of neural networks by enforcing Lipschitz continuity," *Machine Learning*, vol. 110, no. 2, pp. 393–416, 2021.
- [12] G. Khromov and S. P. Singh, "Some fundamental aspects about Lipschitz continuity of neural networks," *arXiv:2302.10886*, 2023.
- [13] H. G. Bock and K.-J. Plitt, "A multiple shooting algorithm for direct solution of optimal control problems," *IFAC Proceedings Volumes*, vol. 17, no. 2, pp. 1603–1608, 1984.
- [14] X. Glorot and Y. Bengio, "Understanding the difficulty of training deep feedforward neural networks," in *Proceedings of the Thirteenth International Conference on Artificial Intelligence and Statistics*. JMLR Workshop and Conference Proceedings, 2010, pp. 249–256.
- [15] T. Wigren and J. Schoukens, "Three free data sets for development and benchmarking in nonlinear system identification," in *2013 European Control Conference (ECC)*. IEEE, 2013, pp. 2933–2938.
- [16] J.-P. Noël and M. Schoukens, "F-16 aircraft benchmark based on ground vibration test data," 4TU.ResearchData," *Dataset*, doi: 10.4121/12954911.
- [17] J. Bradbury, R. Frostig, P. Hawkins, M. J. Johnson, C. Leary, D. Maclaurin, G. Necula, A. Paszke, J. VanderPlas, S. Wanderman-Milne, and Q. Zhang, "JAX: composable transformations of Python+NumPy programs," 2018, <https://github.com/google/jax>.
- [18] M. Hessel, D. Budden, F. Viola, M. Rosca, E. Sezener, and T. Hennigan, "Optax: composable gradient transformation and optimisation, in JAX!" 2020, <https://github.com/deepmind/optax>.
- [19] J. Rader, T. Lyons, and P. Kidger, "Optimistix: modular optimisation in JAX and Equinox," *arXiv:2402.09983*, 2024.
- [20] J. A. Andersson, J. Gillis, G. Horn, J. B. Rawlings, and M. Diehl, "CasADi: a software framework for nonlinear optimization and optimal control," *Mathematical Programming Computation*, vol. 11, pp. 1–36, 2019.